LA-UR- 97-5119

Approved for public release; distribution is unlimited.

Title: STEADY-STATE HNG COMBUSTION MODELING

CONF-980804--

Author(s): J. LOUWERS
G.M.H.J.L. GADIOT
M. Q. BREWSTER
S.F. SON
T. PARR
D. HANSON-PARR

Submitted to: 27TH INTERNATIONAL SYMPOSIUM ON COMBUSTION, UNIVERSITY OF COLORADO AT BOULDER, AUGUST 207, 1998

Los Alamos
NATIONAL LABORATORY

DISCLAIMER

Combustion Symposium
Boulder, CO, August 2-7, 1998

Steady-State HNF Combustion Modeling

J. Louwers* and G.M.H.J.L. Gadiot†, TNO Prins Maurits Laboratory, Rijswijk, The Netherlands,
M.Q. Brewster‡, University of Illinois, Urbana, Illinois, U.S.A.,
S.F. Son§, Los Alamos National Laboratory, Los Alamos, New Mexico, U.S.A.,
T. Parr¶ and D. Hanson-Parr‖, Naval Air Warfare Center, China Lake, California, U.S.A.

Abstract

Two simplified modeling approaches are used to model the combustion of Hydrazinium Nitroformate (HNF, $N_2H_5 \cdot C(NO_2)_3$). The condensed phase is treated by high activation energy asymptotics. The gas phase is treated by two limit cases: the classical high activation energy, and the recently introduced low activation energy approach. This results in simplification of the gas phase energy equation, making an (approximate) analytical solution possible. The results of both models are compared with experimental results of HNF combustion. It is shown that the low activation energy approach yields better agreement with experimental observations (e.g. regression rate and temperature sensitivity), than the high activation energy approach.

Introduction

The modeling of solid propellants may be a cost effective way to determine properties such as regression rates, and temperature sensitivity before even carrying out any experiment. Composite propellants are contemporary workhorses for many applications, but modeling of these *heterogeneous* propellants is very complex. Some models for composite propellant combustion have been developed, such as the PEM model [1]. However, these models require extensive experimental calibration.

It is therefore currently recognized that more complex models are needed, to be able to compute regression rates, and other properties *a-priori*. As starting point for composite propellant models, many models of solid monopropellant combustion were recently developed [2]-[4]. These models are often based on simplified chemical kinetics, coupled with a multi-phase one-dimensional space domain. Due to the extent of these numeric experiments, basic principles are often not revealed.

In this paper, modeling results using simplified approaches are presented. The goal of the models is maximal predictive capability and accuracy, coupled with minimal complexity. This is achieved by using essential physics and chemistry only, yielding tractable models. The condensed phase is treated by a high activation energy approximation method. The gas phase is treated in two ways: the classical high activation energy limit (Denison-Baum-Williams, DBW, model) [5, 6], and the recently introduced low activation energy limit (Ward-Son-Brewster, WSB, model) [7]. Both limits allow for an analytical solution of the gas phase energy equation. The WSB approach was found to match the experimental observations much better than the DBW models for HMX and double base propellants [8].

It is the intention of this work to verify whether the new WSB-approach also gives better results for Hydrazinium Nitroformate Combustion (HNF). HNF is a "new" chlorine-free oxidizer for use in future generation composite propellants [9]. Neat HNF shows self-sustained combustion at pressures above 0.025 MPa.

* Ph.D. Student, Corresponding Author phone: +31-15-2843367, fax: +31-15-2843958, email: louwers@pml.tno.nl
† Research Scientist, Research Group Rocket Technology
‡ Professor of Mechanical Engineering, Department of Mechanical and Industrial Engineering
§ Technical Staff Member, High Explosives Science and Technology Group
¶ Research Chemist, Weapons Division, Research Department
‖ Research Chemist, Weapons Division, Research Department

Model

The combustion of HNF is modeled as a one dimensional, steady state process. The condensed phase is described by a unimolecular, irreversible, zero-order decomposition reaction

$$\mathrm{A} \rightarrow \mathrm{B}\,, \tag{1}$$

where A represents the solid HNF, and B some kind of unstable intermediate species (such as the observed NO_2, HONO and N_2O). B reacts further according to the following bimolecular, irreversible, gas phase reaction

$$\mathrm{B+M} \rightarrow \mathrm{C+M}\,, \tag{2}$$

where C represents intermediate gas phase products, such as NO. M represents unstable species such as N, H and OH. The kinetic scheme represented by Eq.'s (1) and (2) is an ad hoc global description. This model was not derived from a detailed kinetic scheme, but from a conceptual point of view. The above mentioned species represented by B and C are representative for HNF, and help to clarify the idea behind the global description.

The reactions represented by the second step (B+M→C+M) consume the intermediate radical species. These reactions are characterized by high exothermicity and low activation energy barrier. M can be viewed as a pool of unspecified chain carriers, whose mass fraction is constant, and negligibly small compared to the main species B and C [7]. The reaction is second order overall, and first order with respect to B. For purposes of modeling species conservation, no distinction is made between the M species that appear on the left and right hand sides of Eq.(2). The process is assumed to be a bimolecular exchange reaction, which for species bookkeeping purposes, assumes only two gas species, B (reactant) and C (product).

The molecular weights of the various species are assumed to be equal, and mass diffusion in the gas phase is assumed to be described by Fick's law. The specific heat capacity and thermal conductivities are assumed to be constant. The gas phase and condensed phase specific heat capacity are assumed to be equal. To simplify the solution of the gas phase equations, the Lewis number is assumed to be unity, $Le = k_g/\rho_g dc_p = 1$ (for symbols see nomenclature at end of article). The propellant may be illuminated with an external laser heat flux, with radiative energy Q_r (in $\mathrm{W/m^2}$). This heat flux is absorbed in the condensed phase according to Beer's law. Gas phase absorption is assumed to be zero. The gas phase is assumed to obey the ideal gas law. Mass diffusion in the condensed phase is neglected.

Condensed phase

With the above assumptions, the condensed phase is described by the following energy equation

$$mc_p \frac{dT}{dx} = k_c \frac{d^2T}{dx^2} + Q_c \epsilon_c + Q_r K_a \exp(K_a x)\,, \tag{3}$$

with boundary conditions

$$T(0) = T_s\,, \quad \text{and} \quad \lim_{x \rightarrow -\infty} T(x) = T_0\,. \tag{4}$$

As a zero-order condensed phase reaction was assumed, the reaction rate is given by

$$\epsilon_c = \rho_c A_c \exp\left(-\frac{E_c}{RT}\right)\,. \tag{5}$$

It was shown by Von Elbe et al. [11], and Louwers et al. [12] that the condensed phase of HNF has a thin reactive zone, i.e. a high activation energy for the decomposition process as given by Eq.(1). This means that activation energy assymptotics (AEA) may be used to find the solution of Eq.(3). The well known solution is [13, 14]

$$m^2 = \frac{A_c R T_s^2 k_c \rho_c \exp(-E_c/RT_s)}{E_c(c_p(T_s - T_0) - Q_c/2 - f_r Q_r/m))}\,. \tag{6}$$

Gas phase

Solution of the gas phase equations is less straightforward. Most early models are based on the flame sheet approach, i.e. a very thin reactive zone, where all the gas phase heat release occurs. This process is typical for gas phase kinetics with high activation energy ($E_g \rightarrow \infty$). Mathematically the heat release can be described by a Dirac delta function. It was recently argued by Ward et al. that a very low gas phase activation energy ($E_g \rightarrow 0$) is more physical [7]. Their perspective is based on the fact that the temperature profile of HMX could be much better replicated by $E_g = 0$, than $E_g = \infty$. Analogs in gas phase combustion provide further evidence

that such an approach is not unrealistic. Most of the energy of a hydrogen/oxygen system is released during the recombination/termination step, which has a low activation energy barrier [10]. Both limit cases ($E_g = 0$, and $E_g = \infty$) will be discussed here, to see the overall effect on the model.

The energy equation in the gas phase is

$$mc_p \frac{dT}{dx} = k_g \frac{d^2T}{dx^2} + Q_g \epsilon_g \,, \tag{7}$$

with the reaction rate given by

$$\epsilon_g = \rho_g^2 B_g Y T^2 \exp\left(-\frac{E_g}{RT}\right) \,, \tag{8}$$

where Y is the mass fraction of B. The density of the gas phase, ρ_g is found from the ideal gas law. The interface conditions are found from energy conservation at the surface

$$T_s = T_0 + \frac{Q_c}{c_p} + \frac{1}{mc_p}\left[k_g \left(\frac{dT}{dx}\right)_{x=0} + Q_r\right] \,, \tag{9}$$

and

$$T_f = T_0 + \frac{Q_c + Q_g + Q_r/m}{c_p} \,. \tag{10}$$

The species equation of the gas phase is

$$m\frac{dY}{dx} = \rho_g d \frac{d^2Y}{dx^2} - \epsilon_g \,. \tag{11}$$

For the species equation, the boundary conditions are

$$Y_s = 1 + \frac{\rho_g d}{m}\left(\frac{dY}{dx}\right)_{x=0} \,, \tag{12}$$

and

$$\lim_{x\to\infty} Y = 0 \,. \tag{13}$$

Because of the assumption $Le = 1$, the gas phase energy equation, and species equation have identical forms, and can be written as two similar nondimensional equations (nondimensional quantities denoted by *) [7]

$$m^* \frac{dT^*}{dx^*} = \frac{d^2T^*}{dx^{*2}} - D_g(T_f^* - T^*)\exp\left(-\frac{E_g^*}{T^*}\right) \,, \tag{14}$$

and

$$m^* \frac{dY}{dx^*} = \frac{d^2Y}{dx^{*2}} - D_g Y \exp\left(-\frac{E_g^*}{T_f^* - YQ_g^*}\right) \,. \tag{15}$$

The boundary equations transform accordingly. For arbitrary values of E_g^*, Eq.(14) has to be solved iteratively with Eq.(6) to yield T_s^* and m^*. Note that solution of this set requires solution of a 2nd order differential equation. For the two limiting cases, $E_g = 0$, and $E_g \to \infty$, it is possible to obtain an analytical solution.

The first limit is that of a very low activation energy in the gas phase, $E_g \to 0$. For this case an analytical solution of Eq.(14) can be obtained

$$\frac{T^* - T_f^*}{T_s^* - T_f^*} = \exp\left(-\frac{x^*}{x_g^*}\right) \,. \tag{16}$$

In this equation x_g^* is a dimensionless characteristic gas reaction zone thickness, given by

$$x_g^* = \frac{2}{\sqrt{m^{*2} + 4D_g} - m^*} \,. \tag{17}$$

In summary: In the limit of a high condensed phase activation energy, coupled with a low activation energy gas phase, the analytical solution of the problem is given by the (nondimensional) form of Eq.(6)

$$m^{*2} = \frac{A_c^* T_s^{2*} \exp(-E_c^*/T_s^*)}{E_c^*(T_s^* - T_0^* - Q_c^*/2 - f_r J)} \,. \tag{18}$$

This equation is solved simultaneously with Eq.(17) The energy balance is given by the nondimensional result of Eq.(9)

$$T_s^* = T_0^* + Q_c^* + \frac{Q_g^*}{x_g^* m^* + 1} \ . \tag{19}$$

For the high activation energy gas phase ($E_g \to \infty$), the regression rate is given by Williams's gas phase controlled analytical solution (for $E_g/RT_f \gg 1$) [14]

$$m^2 = \frac{2k_g B_g M^2 p^2 c_p T_f^4}{E_g^2 Q_g^2} \exp\left(-\frac{E_g}{RT_f}\right) \ . \tag{20}$$

This expression indicates that the mass flux is determined by gas kinetics only, and not by decomposition kinetics. Note that actually Q_r affects T_f (Eq. (10)), which affects m. For this case the energy balance yields

$$T_s^* = T_0^* + Q_c^* + Q_g^* \exp\left(-x_g^* m^*\right) \ . \tag{21}$$

For the high activation energy limit case, the AEA result, Eq.(18), is still used for the determination of the surface temperature T_s^*. Results of this traditional analytical limit case will be compared with the new concept of $E_g = 0$ to show the overall improvements of the model's predictive capability.

Results

The properties of HNF as used for the calculations are summarized in Table 1. During all calculations these values were held constant. The condensed phase activation energy $E_c = 75\,\mathrm{kJ/mole}$ was found to give good results in the whole pressure range of interest. This value is close to the 84 kJ/mole required to break-up HNF into liquid hydrazine and nitroform. The values of the Arrhenius prefactors, A_c and B_g, were determined from the experimental observation that $T_s = 553\,\mathrm{K}$ and $r_b = 0.77$ mm/s at 0.1 MPa [11, 12]. After this *calibration* of the model at a single burning condition, the regression rate is calculated at different pressures, without modification of any of the other parameters. The thermophysical properties of solid HNF were recently measured [16]. The specific heat capacity and thermal conductivity were found to have a slight temperature dependence. In this model constant values at 100°C are used.

Q_g		2589	kJ/kg
Q_c		−30.0	kJ/kg
A_c		$3.30 \cdot 10^8$	1/s
B_g	$E_g = 0$	$5.71 \cdot 10^{-2}$	$\mathrm{m^3/kgK^2s}$
	$E_g = \infty$	$1.05 \cdot 10^4$	$\mathrm{m^3/kgK^2s}$
c_p		0.97	kJ/kgK
k_g		0.07	W/mK
k_s		0.32	W/mK
E_c		75	kJ/mole
E_g		167	kJ/mole
ρ_c		1860	$\mathrm{kg/m^3}$
M		25.6	kg/kmole

Table 1: Input values used for HNF calculations.

Steady state HNF combustion

Figure 1 shows the results of the calculated regression rate for both models, compared with experimental data (from Ref.[15]). Like most energetic materials, HNF's regression rate can be described by $r_b = ap^n$. The high activation energy limit yields the familiar $n = \frac{\delta}{2} = 1$, whereas $n = 0.89$ was found experimentally for HNF combustion (least-squares fit to all data points in Fig. 1). Because the regression rate was gauged at 0.1 MPa, the flame sheet overpredicts the regression rates above 0.1 MPa. The WSB approach shows good agreement with the experimental results. This model predicts $n = 0.87$ (at 1 MPa).

However above 0.7 MPa, there is a clear difference between the WSB-results and the experimental data. This difference can be attributed to the fact that not only the gas phase kinetics change with pressure, but

also the flame temperature. At 0.1 MPa the flame temperature of HNF is $T_f = 2766\,\mathrm{K}$. When the pressure is increased, the flame temperature of HNF increases considerably, e.g. $T_f = 2949\,\mathrm{K}$ at 1 MPa, and $T_f = 3112\,\mathrm{K}$ at 10 MPa. This is due to the fact that the equilibrium composition is dependent on the pressure. The higher flame temperature results in an extra heat feedback to the surface, not accounted for by the model. This varying flame temperature can be introduced into the model, by varying Q_g as function of pressure, so that the calculated adiabatic flame temperature is reached, $T_f = (Q_g + Q_c)/C_p + T_0$. The rest of the parameters is kept constant. The result is an improved agreement between the WSB-model and the experimental results, see Fig. 2. For reasons of simplicity this modification of the model will not be used throughout the rest of this paper, and from now on constant Q_g values will be used.

Also for low and high initial temperatures, the WSB-model has good agreement with the experimental results, see Fig. 3. This sensitivity of the burning rate to the initial temperature, is defined by the following expression

$$\sigma_p = \frac{1}{r_b}\left(\frac{\partial r_b}{\partial T_0}\right)_p . \tag{22}$$

By determining the regression rate at 292 K and 293 K HNF's temperature sensitivity was determined for both the DBW and the WSB model, see Fig. 4. This graph also shows the experimental determined temperature sensitivity from the data points of Fig. 3. This is done in two ways: First, *direct* determination of σ_p at each pressure by a fit of $\ln(r_b)$ vs. temperature. The second method is by a least-squares power laws fit to the regression rate curves at each pressure. Then the temperature sensitivity is determined from the differences between these fits at each pressure. If the propellant burns nicely according to $r_b = ap^n$, then the second method will give more accurate results.

From Fig. 4 it is seen that the low activation energy limit predicts a pressure dependence of the temperature sensitivity. This limit case shows reasonable agreement with the direct determined values for σ_p. The agreement with the temperature sensitivity as determined by the second method is very good. The $E_g \to \infty$ model is not capable of capturing a pressure variation of σ_p. Unfortunately the large errors from the direct method make it impossible to favor one of the two modeling approaches. The temperature sensitivity as determined from fitting power laws first, is much better for the WSB-approach, then for the DBW-model.

Recently a kinetical model for HNF combustion was developed [17]. This model belongs to the group of numerical models already mentioned in the introduction. The solid to gas interface is fixed at the origin, by specification of the surface temperature. This then yields the mass flux as an eigenvalue of the system of governing equations [3]. A limited set of global decomposition reactions is allowed to take place in the condensed phase. The gas phase is modeled by Yetter's RDX gas phase mechanism [18], with added reactions for HNF decomposition. Typical products formed at the surface are $HNF_{(g)}$, CO, N_2O, HONO and N_2H_4.

Figure 5 compares the temperature profile as found from both limit cases, and this detailed modeling. It is seen that the temperature profile of the simplified WSB-model is close to that of the detailed chemical model. Both simplified models show a temperature profile close to the final flame temperature at $x = 1\,\mathrm{mm}$. The detailed calculations show a lower temperature due to the slow NO reactions, similar to the "dark-zone" in double-base propellants. With a second step in the gas phase, C $\to$ D, the simple models would also be able to calculate this intermediate zone. The final flame temperature of the kinetical model is equal to that of the other models. It was determined by NO UV-absorption experiments that temperatures close to the adiabatic flame temperature are reached within 1 mm above the surface [12]. All three modeling approaches confirm this. However, the accuracy of these experiments does not allow to reject one of the models.

A closer agreement between the temperature profile of WSB/DBW-models and the kinetic model is obtained by using the intermediate temperature of 2550 K as the final temperature. It was verified that after re-calibration of the WSB-model the effect is small. For the DBW-model there is no effect, as a decrease of Q_g is compensated by a decrease of B_g (see Eq.(20)). These results will therefore not be discussed here.

Figure 6 shows the position where 63% ($= x_g$) and 99% of the final flame temperature are reached. These positions are characteristic dimensions for the gas phase reaction zone thickness. In the figure this flame thickness is compared to several experimental results. The flame standoff distances in Fig. 6 were obtained from video images as the distance off the surface of the CN chemiluminiscent emission. The CN profile peak location was determined by planar laser induced fluorescence (PLIF), which is a more accurate determination of the CN standoff. The CN profile peak do not necessarily coincide with x_g, but should at least follow the same trend, and be of the same order of magnitude. The magnitude is much better predicted by the WSB-model. The DBW-model flame thickness is an order of magnitude too thin (as also the case for HMX). It is seen that both the DBW and WSB-models predict the experimental observed pressure dependence (nearly $1/p$).

Laser-assisted combustion

As part of the study of the transient combustion of HNF, Finlinson determined the laser assisted regression rates of HNF [19]. This data allows the further validation of the model. No absorption or reflection measurements have been carried out for HNF in the 10.6 μm CO_2-laser range used by Finlinson. Two values for the absorption coefficient will be used here: high absorption, $K_a = 5000\,\mathrm{cm}^{-1}$, and very low absorption, $K_a = 300\,\mathrm{cm}^{-1}$. This low absorption value was recently proposed as a good value for HNF, based on Finlinson's transient data. The reflection coefficient is determined from a best fit to all experimental data. From the previous section, it has become clear that the low activation energy limit, WSB, shows best agreement with the experiments. Therefore only this model will be discussed here.

Figure 7 shows the laser-assisted combustion of HNF. For all pressures the models predict the sensitivity to the external laser heat flux in good agreement with the experimental data. The difference between experiments and the modeling is caused by the small inaccuracies of the model, already at $Q_r = 0$. For these calculations a surface reflection of 60% was used. This value is comparable to the values used for HMX modeling [20]. This work indicates a surface reflectivity of 50%. Neat HMX samples show only 15% reflectivity at room temperature. Several explanations for this difference can be given: ions present in the melt layer, enhanced scattering inside the melt layer due to bubbles, or enhanced absorption at the burning surface due to the presence of decomposition products (hence increased reflectivity). If the pressure increases the melt thickness decreases. This implies a lower reflection. The measurements at 0.6 MPa seem to indicate this. However, the number of measurements at this pressure are limited. Note that the effect of the value of K_a is very small.

Conclusions

Two very simple models for the combustion of HNF have been presented. The gas phase has been calculated by two limit approaches: low (WSB) and high (DBW) gas phase activation energy. The WSB approach shows great predictive capability, in both laser-assisted and self-sustained regression rates, and temperature sensitivity. The agreement of these propellant properties is much better than with the usual assumption of large gas phase activation energy (DBW). By introducing HNF's strong pressure dependent adiabatic flame temperature into the WSB-model even better results are obtained.

Nomenclature

Symbols

A	Arrhenius prefactor
B	Arrhenius prefactor
c_p	Specific heat capacity
D_g	Damkohler number
d	Diffusion coefficient
E	Activation energy
f_r	fraction of Q_r absorbed below surface reaction zone, $\exp(-K_a x_R)$
K_a	Absorption coefficient
k	Thermal conductivity
Le	Lewis number
M	Molecular weight
m	Mass flow rate
n	Pressure exponent
Q	Heat release
Q_r	Radiant heat flux
R	Universal gas constant
r_b	HNF regression rate
T	Temperature
x	Space coordinate
x_R	reaction zone length scale, $(k_c/(\rho_c c_p r_b))/(E_c/(2RT_s))$
Y	Mass fraction
α	Thermal diffusivity
δ	Reaction order
ϵ	Chemical reactivity
ρ	Density

Sub- and superscripts

c	Condensed phase
f	Final
g	Gas phase
ref	Reference value
s	Surface
0	Initial
$*$	Nondimensional parameter

Nondimensional quantities

$$D_g = k_g B_g p^2 M^2/((m_{ref} R)^2 c_p)$$
$$E^* = E/(R(T_f - T_0))$$
$$J = Q_r/(c_p m(T_s - T_0)$$
$$m^* = m/m_{ref}$$
$$Q^* = Q/(c_p(T_f - T_0))$$
$$T^* = T/(T_f - T_0)$$
$$x^* = x/(k_g/(m_{ref} c_p))$$

Acknowledgments

SFS is sponsored by Los Alamos National Laboratory which is supported by the U.S. Department of Energy under contract number W-7405-ENG-36. TP and DHP are sponsored under contract number N0001495WX20018 with the Office of Naval Research, Scientific Officer Dr. Richard Miller. The authors would like to thank Jerry Finlinson from Naval Air Warfare Center, China Lake for providing the experimental data, and the helpful discussions.

References

[1] Condon, J.A. and Osborn, J.A., "The Effect of Oxidizer Particle Size Distribution on the Steady and Nonsteady Combustion of Composite Propellants," Air Force Rocket Propulsion Lab, Report No. AFRPL-TR-78-17, 1978.

[2] Liau, Y.C. and Yang, V., "Analysis of RDX Monopropellant Combustion with Two-Phase Subsurface Reactions," *J. Prop. Power* 11:729-739 (1995).

[3] Prasad, K., Yetter, R.A. and Smooke, M.D., "An Eigenvalue Method for Computing the Burning Rates of RDX Propellants," *Comb. Sci. Techn.* 124:35-82 (1997).

[4] Davidson, J. and Beckstead, M., "Improvements to RDX Combustion Modeling," AIAA Paper No. 96-0885, 1996.

[5] Denison, M.R. and Baum, E., "A Simplified Model of Unstable Burning in solid Propellants," *ARS J.* 31:1112-1122 (1961).

[6] Williams, F.A., "Quasi-Steady, Gas-Phase Flame Theory in Unsteady Burning of a Homogeneous Solid Propellant," *AIAA J.* 11:1328-1330 (1973).

[7] Ward, M.J., Son, S.F. and Brewster, M.Q., "Steady Deflagration of HMX with Simple Kinetics A Gas Phase Chain Reaction Model," submitted to *Combust. Flame* (1997).

[8] Brewster, M.Q., Ward, M.J. and Son, S.F., "New Paradigm for Simplified Combustion Modeling of Energetic Solids: Branched Chain Gas Reaction," AIAA Paper No. 97-3333, 1997.

[9] Schöyer, H.F.R., Schnorhk, A.J., Korting, P.A.O.G., Lit, P.J. van, Mul, J.M., Gadiot, G.M.H.J.L. and Meulenbrugge, J.J., "Development of Hydrazinium Nitroformate Based Solid Propellants," *J. Prop. Power* 11:856-859 (1995).

[10] Zeldovich, Ya. B., "Chain Reactions in Hot Flames - an Approximate Theory of Flame Velocities," *Kinetika i Kataliz* 2:305-318 (1961).

[11] Elbe, G. von, Friedman, R., Levy, J.B. and Adams, S.J., "Research on Combustion in Solid Rocket Propellants: Hydrazine Nitroform as a Propellant Ingredient," Atlantic Research Corp., Technical Report No. DA-36-034-AMC-0091R, 1964.

[12] Louwers, J., Parr, T. and Hanson-Parr, D., Unpublished Results, 1997.

[13] Lengelle, G., "Thermal Degradation Kinetics and Surface Pyrolysis of Vinyl Polymers", *AIAA J.* 8:1989-1998 (1970).

[14] Ibiricu, M.M. and Williams, F.A., "Influence of Externally Applied Thermal Radiation on the Burning Rates of Homogeneous Solid Propellants," *Combust. Flame* 24:185-198 (1975).

[15] Atwood, A.I., Boggs, T.L., Curran, P.O., Parr, T.P., Hanson-Parr, D., Wiknich, J. and Price, C.F., "Burn Rate Temperature and Pressure Sensitivity of Solid Propellant Ingredients," *Int. Workshop Combustion Instability of Solid Propellants and Rocket Motors,* Politechnico di Milano, Italy, 16-18 June 1997.

[16] Hanson-Parr, D., Parr, T.P., "Measurements of Solid Rocket Propellant Oxidizers and Binder Materials as a Function of Temperature," submitted to *J. Energ. Mat.* (1997).

[17] Louwers, J, "A Model for HNF Monopropellant Combustion: First Results," TNO Prins Maurits Laboratory, Report No. PML 1996-C92, 1996.

[18] Yetter, R.A., Dryer, F.L., Allen, M.T. and Gatto, J.L, "Development of Gas-Phase Reaction Mechanisms for Nitramine Combustion," *J. Prop. Power* 11:683-697 (1995).

[19] Finlinson, J.C., "Laser Recoil Combustion Response of HNF Oxidizer from 1 to 6 atm," AIAA Paper No. 97-3342, 1997.

[20] Loner, P.S. and Brewster, M.Q., "Oscillatory Laser-Induced Combustion of HMX," *1997 JANNAF Combustion Meeting, CPIA,* West Palm Beach, FL., Oct. 1997.

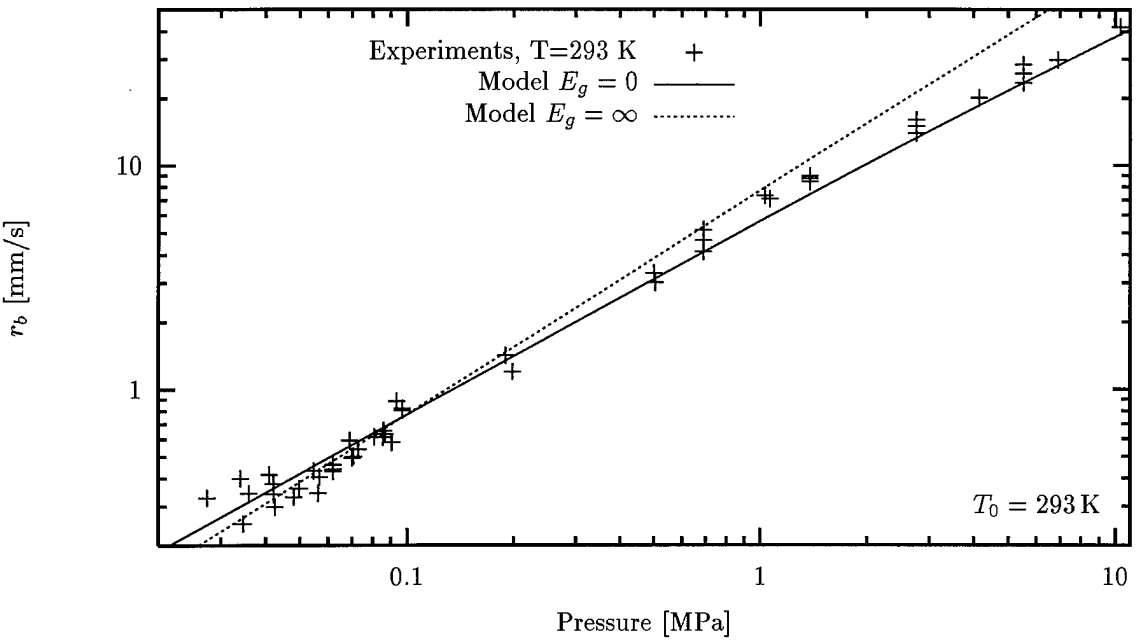

Figure 1: Comparison of calculated and measured regression rate of neat HNF samples.

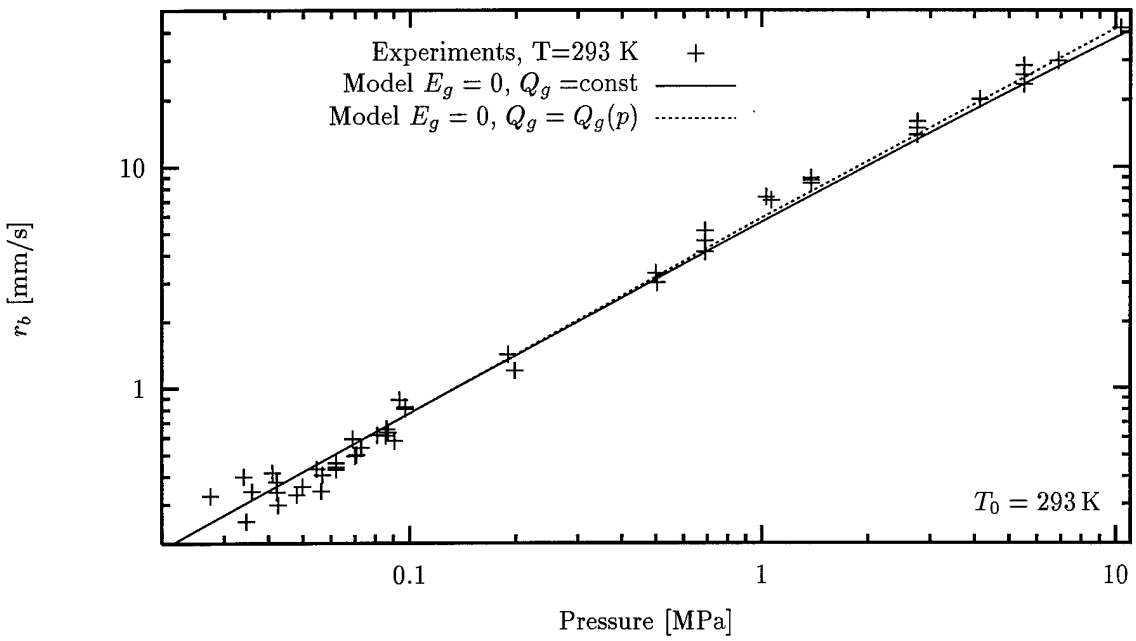

Figure 2: Effect of introducing pressure dependent Q_g to account for the varying flame temperature with pressure.

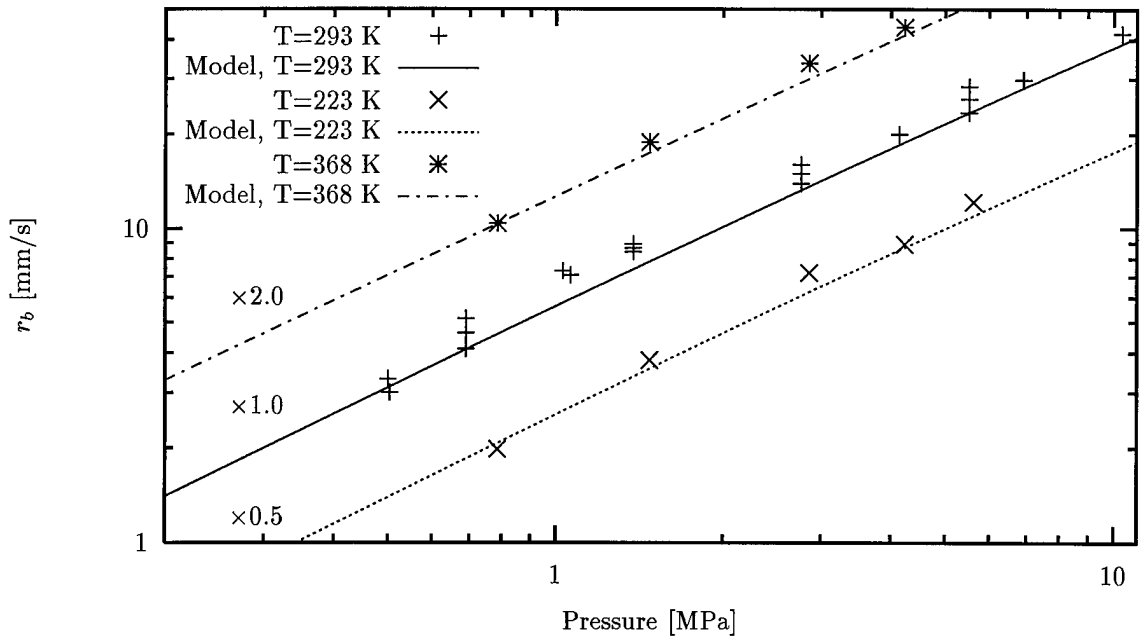

Figure 3: Comparison of calculated (WSB-model) and measured regression rate of neat HNF samples. (Note the multiplication factors, which are introduced to prevent overlap of data.)

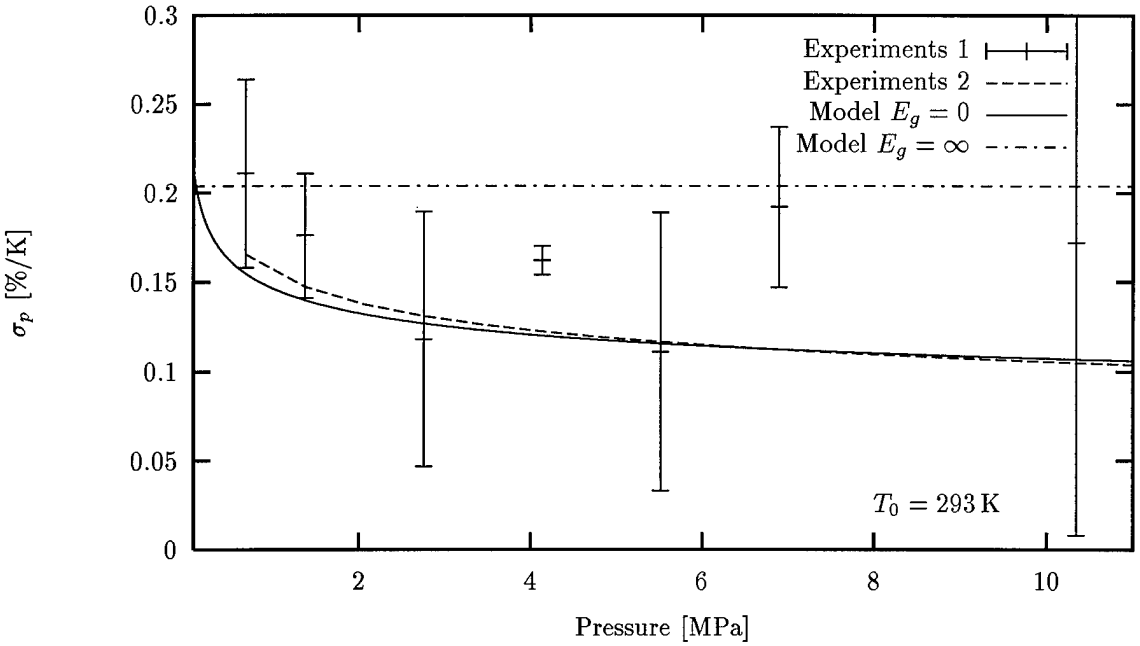

Figure 4: Experimental vs. theoretical temperature sensitivity of HNF for both modeling approaches (errorbars indicate the standard deviation from the $\ln(r_b)$ vs. T fit). For explanation of the two different methods of experimental σ_p evaluation see the text. Within the $E_g = \infty$ approach only a constant temperature sensitivity is calculated, $\sigma_p = (T_f + E_g/2RT_f)/T_f$.

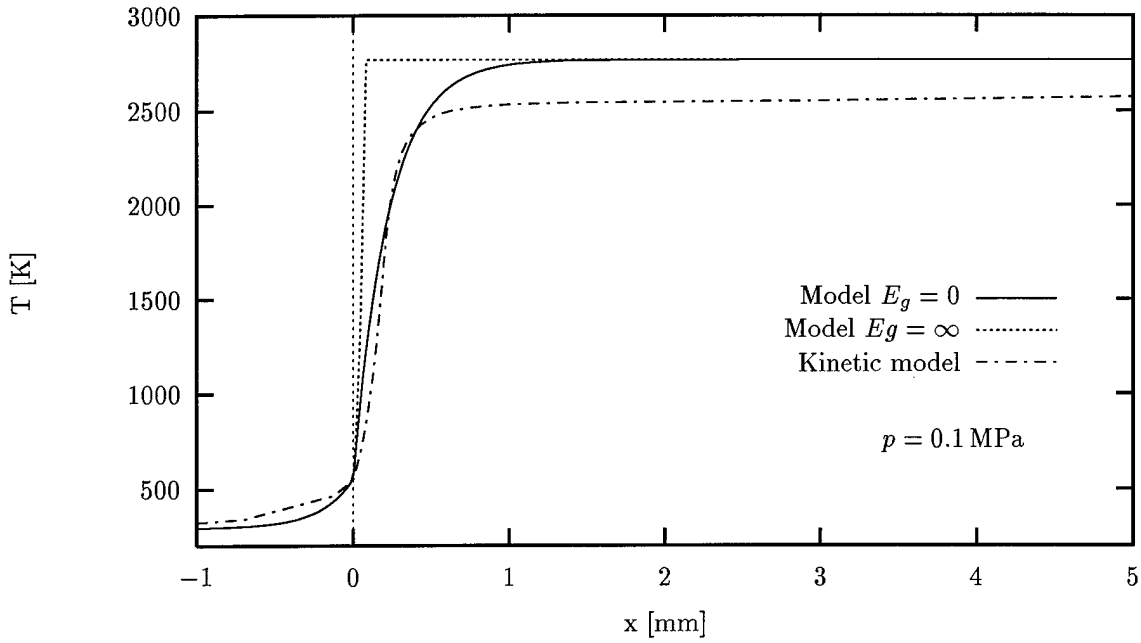

Figure 5: Temperature profile of HNF for both limit models, and a comprehensive detailed kinetical model.

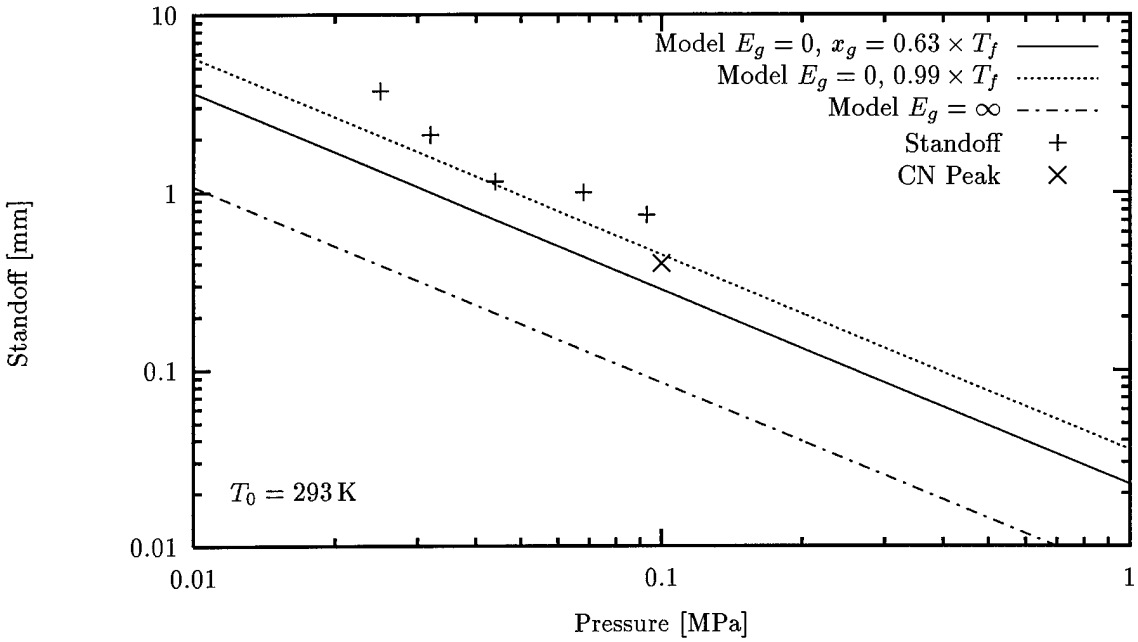

Figure 6: Flame standoff distance as calculated from both models, compared with experimental determined flame standoff (height above the burning surface of CN chemiluminiscence), and CN profile peak position (as determined by planar laser induced fluorescence).

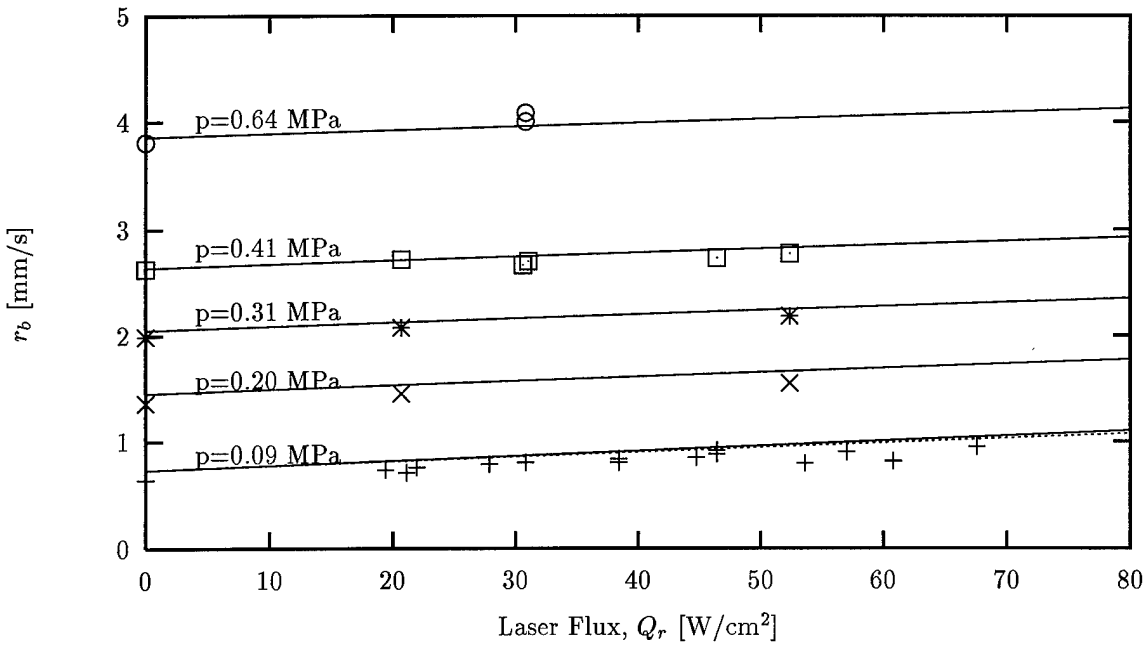

Figure 7: Laser-assisted regression rates of HNF at different pressures. Points: experimental data; Solid lines: WSB-model's results for $K_a = 300\,\mathrm{cm}^{-1}$; Dotted line: WSB-models result for $K_a = 5000\,\mathrm{cm}^{-1}$. The WSB model predicts HNF's sensitivity to an external heat source accurately for all pressures. The deviation from the experimental results is caused by the difference between the model and the experiments, already at $Q_r = 0$.

Report Number (14) LA-UR-97-5119
CONF-980804--

Publ. Date (11) 19980[illegible]
Sponsor Code (18) DOE/DP, DOE/DP, XF
UC Category (19) UC-706, UC-741, DOE/ER

DOE